Journal of Engineering Physics and Thermophysics, Vol. 73, No. 1, 2000

MATHEMATICAL MODELS OF RADIATIVE-CONDUCTIVE HEAT EXCHANGE IN HEAT-SHIELD MATERIALS OF SHUTTLE SPACE TRANSPORTATION SYSTEMS

S. V. Reznik

UDC 629.7.018.3:536.24+536.33

A system of mathematical models of radiative-conductive heat exchange in partially transparent porous heat-shield materials is considered.

Distinctive Features of Reusable Heat Shield. An increasing role in outer space exploration is being assigned to shuttle space transportation systems (SSTSs) such as rockets, aerospaceplanes (spacecraft-aircraft), aerospace rocket complexes, and interorbital transport aerobraking vehicles. Of special importance for SSTSs are the problems of thermal protection [1-5], since the surfaces being protected extend to hundreds of square meters, and intense heating during motion in the earth's atmosphere lasts several thousands of seconds. Undesirable phenomena in heat shields (HSs) of SSTSs are melting, ablation, shrinkage, bulging, and other transformations promoting irreversible alteration of aerodynamic and thermal protection characteristics. Even the first SSTSs such as the Space Shuttle and Buran spacecraft required protection of the load-bearing structure with an area of about 1000 m^2 for 100 flights with high thermal loadings acting for about 2000 sec [2, 4, 5], which precluded the possibility of using heavy HSs with fillers from asbestos, glass, or carbon fabrics impregnated with a polymer binder.

Of the many types of thermally stable HSs, tiling and flexible heat shields have been mastered; investigations of skins with a carrying body are being continued. Common to the first two types is local coupling of the skin with the load-bearing structure; in the third case there is an organic unity between the heat-shield and load-bearing structures. All the above types of HSs are combined by blocking heat transfer into the load-bearing structure by means of thermally stable insulators with a surface of low catalytic activity and reradiation of excess energy to the surrounding space.

Stringent requirements for materials to be used in HSs of SSTSs are met by materials made of SiO_2 and Al_2O_3 fibers that have a porosity of more than 90% and exhibit high thermal and chemical resistance. The fibers forming these materials are partially transparent both to the external radiation sources and the intrinsic source in the visible and partially infrared bands. In these materials, energy is transferred simultaneously by heat conduction, radiation, and convection, with the predominance of radiative-conductive heat exchange (RCHE), and there are no physicochemical transformations in the operating range of temperatures.

Mathematical Models of Radiative-Conductive Heat Exchange in Heat Shields. Important aspects of simulation of radiative-conductive heat exchange in HSs have already received their treatment in the literature [6-12], but the exceptional complexity of the problem requires a comprehensive application of the methods of mathematical simulation, physical modeling, and of parametric identification [13].

The HSs of SSTSs combine elements manufactured of diversified materials; they fulfill different functions and are interrelated by a single purpose. A systems approach allows one to consider HSs as complex engineering systems, i.e., as objects with a hierarchical structure, and to single out separate structural components by objectively existing properties and investigation tasks. It is customary to divide the components of the complex engineering systems into substructures and elements. For example, the Buran structure can involve a substructure of tiling heat shield. This substructure admits, in turn, of further division into elements, namely,

N. É. Bauman Moscow State Technical University, Moscow, Russia. Translated from Inzhenerno-Fizicheskii Zhurnal, Vol. 73, No. 1, pp. 11-25, January–February, 2000. Original article submitted September 14, 1999.

1062-0125/2000/7301-0009$25.00

TABLE 1. "CAR" Software Package to Model RCHE Processes

Shape of the object	Simulated phenomena and factors	Applications
Infinitely extended plate, solid or hollow cylinder	Nonstationary one-dimensional RCHE Uniform heating by diffuse and/or directional radiation Convective heat exchange and removal of heat by radiation in the opaque region of material on side surfaces Volumetric absorption and scattering of radiation Temperature dependence of TPPs; temperature and spectral dependence of OPs	Evaluations of thermal regimes for variations in TPPs and OPs of materials under field and model conditions
Multilayer plate	Same as in the model of an infinitely extended plate with arbitrary alternation of opaque and partially transparent materials	Selection of dimensions and properties of individual layers
Plate of limited dimensions with inclusions	Two-dimensional RCHE Nonuniform, time-variable heating by diffuse and/or directional radiation Asymmetric convective heat exchange and removal of heat by radiation in the opaque region of the material on the sides of the layer Volumetric absorption and scattering of radiation Temperature dependence and anisotropy of TPP; temperature and spectral dependence of OP Dimensions and physical properties of inclusions	Analysis of procedural error of contact probes of temperature Selection of dimensions when planning thermal tests

heat protective tiles, temperature compensators, and adhesive-bonded joints. Each tile can be considered as an element consisting of an erosion-resistant coating and a layer of fibrous heat insulation. Needless to say, this level of decomposition is far from being final.

Decomposition of any complex structures may yield substructures possessing topological generality: multilayer plates, multilayer jackets, and rod systems, and at a lower level these are canonically shaped elements such as plates, shells, and rods. The topological generality implies a possibility of calculating the temperature state of all elements of the same type by certain standard methods.

Not only in thermal physics, but also in other fields of science, is the process of developing computational schemes poorly formalized; it is iterative and in many respects determined by the experience and intuition of a researcher. This results in the multivariance of computational schemes for identical physical objects that is generated both by the different level of structural decomposition and diversity of statements, methods, and algorithms for one-level objects of structural decomposition. Logic prompts that the hierarchical system of computational schemes must be adequate to the hierarchical system of standard substructures and elements, and the multivariance of methods and algorithms must be combined with reasonable universality. It is appropriate to have unified methods of mathematical description – the same types of models, methods, and algorithms of problems solution, a unified representation of data on thermophysical (TPPs) and optical properties (OPs) of materials – in the system of computational schemes. This facilitates testing of more complex problems by artificial reduction of their dimensions and cuts down expenditures on software development.

The modern form of constructing the hierarchical system of computational schemes for a topically isolated range of problems is an application package. Statements and algorithms of solving direct RCHE problems that form the functional part of the "CAR" software package, developed at the N. E. Bauman Moscow State Technical University, are oriented to simulating the temperature state of the HSs of SSTSs from partially transparent scattering materials (Table 1). Among basic assumptions of the mathematical models realized in the "CAR" package, we will take note of the assumption about a negligibly small role of convection in overall heat transfer. In the first place it is valid for HSs of porous materials, in which pressure filtration of a cooler is absent [7].

Infinitely extended plate and solid or hollow cylinders (Figs. 1 and 2):

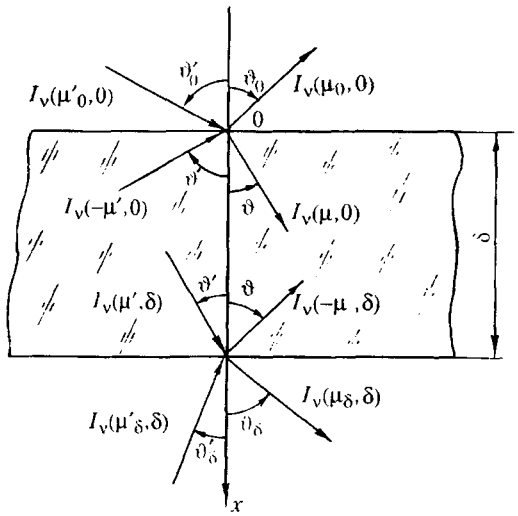

Fig. 1. Model of radiative-conductive heat exchange in an infinitely extended plate.

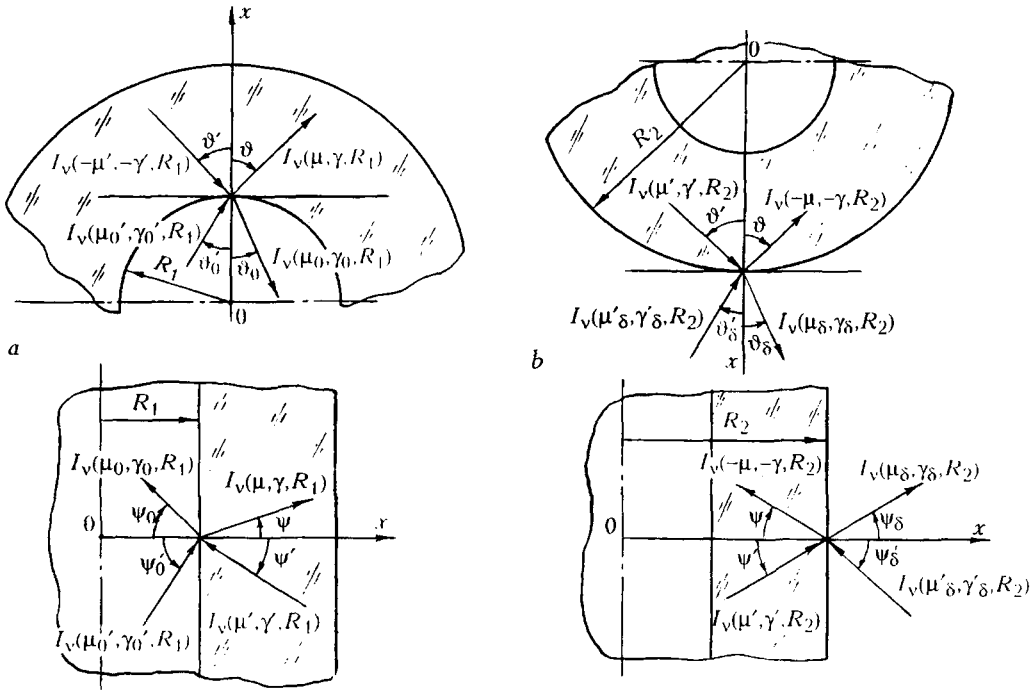

Fig. 2. Model of radiative-conductive heat exchange in an infinitely extended solid or hollow cylinder: a) inner surface of the cylinder; b) its outer surface.

$$C(T)\frac{\partial T}{\partial \tau}=\frac{1}{x^{\bar{n}}}\frac{\partial}{\partial x}\left(x^{\bar{n}}\lambda(T)\frac{\partial T}{\partial x}\right)+q_\nu(x,\tau); \tag{1}$$

$$\tau=0 \quad T=T_0(x); \tag{2}$$

$$x=0\vee R_1\ (x=\delta\vee R_2)\ (\mp)\ \tilde{K}_{1(2)}\lambda(T)\frac{\partial T}{\partial x}=(\tilde{K}_{1(2)}-1)\,T+\tilde{\varphi}_{1(2)}; \tag{3}$$

a) for the plate (Fig. 1) $0 < x < \delta$ and $-1 \leq \mu \leq 1$:

$$\mu \frac{dI_\nu(\mu)}{dx} = -(\alpha_\nu + \beta_\nu) I_\nu(\mu) + \alpha_\nu n_\nu^2 \frac{B_\nu(T)}{\pi} + \frac{\beta_\nu}{2} \int_{-1}^{1} \tilde{\rho}_\nu(\chi) I_\nu(\mu') d\mu' ; \tag{4}$$

$$x = 0 \quad I_\nu(\mu) = \int_0^1 \tilde{r}_{w1,\nu}(\mu, -\mu') I_\nu(-\mu') d\mu' + \int_0^1 \tilde{q}_{w1,\nu}(\mu, \mu_0') I_\nu(\mu_0') d\mu_0' +$$

$$+ \varepsilon_{w1}(\mu) \frac{B_{w1,\nu}(T)}{\pi} ; \tag{5}$$

$$x = \delta \quad I_\nu(-\mu) = \int_0^1 \tilde{r}_{w2,\nu}(-\mu, \mu') I_\nu(\mu') d\mu' + \int_0^1 \tilde{q}_{w2,\nu}(-\mu, \mu_\delta') I_\nu(\mu_\delta') d\mu_\delta' +$$

$$+ \varepsilon_{w2}(-\mu) \frac{B_{w2,\nu}(T)}{\pi} , \tag{6}$$

where

$$q_\nu = -\frac{\partial}{\partial x} \int_{\bar{\nu}_t} q_{r,\nu} d\nu ; \quad q_{r,\nu} = 2\pi \int_{-1}^{1} I_\nu(\mu) \mu d\mu ;$$

b) for the solid and hollow cylinders (Fig. 2) $0 < x < R \vee R_1 < x < R_2$; $-1 \leq \mu \leq 1$; $0 \leq \gamma \leq 1$:

$$\sqrt{1-\gamma^2} \left(\mu \frac{\partial I_\nu(\mu, \gamma)}{\partial x} + \frac{1-\mu^2}{x} \frac{\partial I_\nu(\mu, \gamma)}{\partial \mu} \right) = -(\alpha_\nu + \beta_\nu) I_\nu(\mu, \gamma) +$$

$$+ \alpha_\nu n_\nu^2 \frac{B_\nu(T)}{\pi} + \frac{\beta_\nu}{2} \int_{-1}^{1} \frac{d\mu'}{\sqrt{1-(\mu')^2}} \int_0^1 \tilde{\rho}_\nu(\chi) I_\nu(\mu', \gamma') d\gamma' ; \tag{7}$$

$$x = 0 \vee R_1 \quad I_\nu(\mu, \gamma) = \int_0^1 \frac{d\mu'}{\sqrt{1-(\mu')^2}} \int_0^1 \tilde{r}_{w1,\nu}(\mu, \gamma, -\mu', -\gamma') I_\nu(-\mu', -\gamma') d\gamma' +$$

$$+ \int_0^1 \frac{d\mu_0'}{\sqrt{1-(\mu_0')^2}} \int_0^1 \tilde{q}_{w1,\nu}(\mu, \gamma, \mu_0', \gamma_0') I_\nu(\mu_0', \gamma_0') d\gamma_0' + \varepsilon_{w1,\nu}(\mu, \gamma) \frac{B_{w1,\nu}(T)}{\pi} ; \tag{8}$$

$$x = R \vee R_2 \quad I_\nu(-\mu, -\gamma) = \int_0^1 \frac{d\mu_0'}{\sqrt{1-(\mu_0')^2}} \int_0^1 \tilde{r}_{w2,\nu}(-\mu, -\gamma, \mu', \gamma') I_\nu(\mu', \gamma') d\gamma' +$$

$$+ \int_0^1 \frac{d\mu_\delta'}{\sqrt{1-(\mu_\delta')^2}} \int_0^1 \tilde{q}_{w2,\nu}(-\mu, -\gamma, \mu_\delta', \gamma_\delta') I_\nu(\mu_\delta', \gamma_\delta') d\gamma_\delta' + \varepsilon_{w2,\nu}(-\mu, -\gamma) \frac{B_{w2,\nu}(T)}{\pi} , \tag{9}$$

where

$$q_\nu = -\frac{1}{x}\frac{\partial}{\partial x}\left(x\int\limits_{\bar\nu_t} q_{r,\nu}\,d\nu\right);\quad q_{r,\nu} = 4\int\limits_{-1}^{1}\frac{\mu d\mu}{\sqrt{1-\mu^2}}\int\limits_{0}^{1} I_\nu(\mu,\gamma)\sqrt{1-\gamma^2}\,d\gamma .$$

In the general case of mixed boundary conditions

$$\tilde\varphi = \tilde\varphi(T,\tau) = \int\limits_{\bar\nu_0} A_{w1(2)}\,q_{w,r}(\tau) - \int\limits_{\bar\nu_0}\varepsilon_{w1(2)}\,B_{w1(2),\nu}(T)\,d\nu - \alpha_{f1(2)}\left(T_{w1(2)}(\tau) - T_{f1(2)}\right).$$

Direct integration of Eqs. (4)-(6) and (7)-(9) presents considerable difficulties; moreover, in order to close systems (1)-(6) and (1)-(3), (7)-(9) through q_ν, it is sufficient to know the densities of the heat flux $q_{r,\nu}$, averaged over angular coordinates, rather than the spectral intensities $I_\nu(\mu)$ or $I_\nu(\mu, \gamma)$. Therefore, for the solution of the radiation transfer equation in the "CAR" package the method of moments [14] is used, which has a fairly high accuracy in describing integral characteristics of radiative heat exchange. Using the two-term approximation of the method of moments [15, 16], problem (4)-(9) can be brought to the form

$$\frac{1}{x^{\bar n}}\frac{\partial}{\partial x}\left(\frac{x^{\bar n}}{\kappa_\nu}\frac{dM_{0,\nu}}{dx}\right) - 3\alpha_\nu M_{0,\nu} = -3\alpha_\nu B^*_\nu(T); \tag{10}$$

$$x = 0 \vee R_1\ (x = \delta \vee R_2)\quad (\mp)\frac{1}{2\kappa_\nu}\left(\frac{1}{3} + \tilde R_{11,w1(2)}\right)\frac{dM_{0,\nu}}{dx} + \frac{1}{2}\left(\frac{1}{2} - \tilde R_{01,w1(2)}\right)M_{0,\nu} =$$

$$= q_{w1(2),r}(\tau)\left(2\eta^{d}_{w1(2)}\,\tilde Q_{01,w1(2)} + \eta^{s}_{w1(2)}\,\tilde Q_{1,w1(2)}\right) + 2\tilde E_{w1(2)}\,n_\nu^2\,B_{w1(2)}(T), \tag{11}$$

where

$$q_\nu = \int\limits_{\bar\nu_t}\alpha_\nu\left(M_{0,\nu} - B^*_\nu(T)\right)d\nu;\quad M_{0,\nu} = \int\limits_{4\pi} I_\nu\,d\Omega$$

is the moment of zero-order radiation intensity having the meaning of radiation intensity averaged over the solid angle Ω; $\tilde R_{\tilde m,\tilde n}$, $\tilde Q_{\tilde m,\tilde n}$, $\tilde Q_{\tilde m}$, and $\tilde E$ are the integral optical characteristics of boundary surfaces [16]:

$$\tilde R_{\tilde m\tilde n} = \int\limits_0^1 \mu^{\tilde n}\,d\mu\int\limits_0^1 \tilde r(\mu,\mu')\,(\mu')^{\tilde m}\,d\mu';\quad \tilde Q_{\tilde m\tilde n} = \int\limits_0^1 \mu^{\tilde n}\,d\mu\int\limits_0^1 \tilde q(\mu,\mu_0')\,(\mu_0')^{\tilde m}\,d\mu_0';$$

$$\tilde Q_{\tilde m} = \int\limits_0^1 \tilde q(\mu,\mu_0^{'s})\,(\mu_0^{'s})^{\tilde m}\,d\mu_0^{'s};\quad E = \int\limits_0^1 \varepsilon(\mu)\,\mu d\mu .$$

The structure of integral optical characteristics depends on the type of boundary surfaces. So, for a plate with mirror surfaces

$$\tilde R_{11} = \int\limits_{\mu^*}^1 \bar R(\mu)\,\mu^2 d\mu + \mu^{*3}/3;\quad \tilde R_{01} = \int\limits_{\mu^*}^1 \bar R(\mu)\,\mu d\mu + \mu^{*2}/2;$$

$$\tilde{Q}_{01} = \int_0^1 (1 - \bar{R}(\mu_0')) \mu_0' d\mu_0' ; \quad \tilde{Q}_1 = (1 - \bar{R}(\mu_0^{'s})) \mu_0^{'s},$$

where the reflection factors $\bar{R}(\mu)$, $\bar{R}(\mu_0')$, and $\bar{R}(\mu_0^{'s})$ are calculated from Fresnel's formulas:

$$\text{for } \mu^* \le \mu \le 1 \quad \bar{R}(\mu) = \frac{1}{2}\left(\frac{\mu_0' - n\mu}{\mu_0' + n\mu}\right)^2 \left(1 + \left(\frac{\mu\mu_0' - n(1-\mu^2)}{\mu\mu_0' + n(1-\mu^2)}\right)^2\right);$$

$$\mu_0' = \sqrt{1 - n^2 (1-\mu)_0} ;$$

$$\text{for } 0 \le \mu_0' \le 1 \quad \bar{R}(\mu_0') = \frac{1}{2}\left(\frac{\mu_0' - n\mu}{\mu_0' + n\mu}\right)^2 \left(1 + \left(\frac{\mu\mu_0' - n(1-\mu^2)}{\mu\mu_0' + n(1-\mu^2)}\right)^2\right),$$

$$\mu = \sqrt{\left(1 - \frac{1 - (\mu_0')^2}{n^2}\right)},$$

and to calculate $\bar{R}(\mu_0^{'s})$ in the latter formula, it is sufficient to replace μ_0' by $\mu_0^{'s}$.

As regards diffuse surfaces, an assumption about the equality of reflection factors in all of the directions is introduced. For example, for a plate with a diffuse surface

$$\tilde{R}_{11} = \int_0^1 \bar{R}^{\mathrm{d}}(\mu')(\mu')^2 d\mu' ; \quad \tilde{R}_{01} = \int_0^1 \bar{R}^{\mathrm{d}}(\mu')\mu' d\mu' ;$$

$$\tilde{Q}_{01} = \int_0^1 (1 - \bar{R}^{\mathrm{d}}(\mu_0'))(\mu_0')^2 d\mu_0' ; \quad \tilde{Q}_1 = (1 - \bar{R}^{\mathrm{d}}(\mu_{0(\delta)}'))\mu_{0(\delta)}' .$$

The incident radiation flux density is connected with the intensity by the expression

$$q_{\mathrm{w1(2),r}} = 2\pi \int_0^1 I(\mu_{0(\delta)}')\mu_{0(\delta)}' d\mu_{0(\delta)}' ,$$

with

$$I(\mu_{0(\delta)}') = I^{\mathrm{d}} \sum_{j=1}^{J} b_j (\mu_{0(\delta)}')^{j-1} + I^{\mathrm{s}} \tilde{\delta}(\mu_{0(\delta)}' - \mu_{0(\delta)}^{'s}) .$$

In the formulas given above, the frequency subscript ν is omitted to simplify representation. The multigroup approximation [17] is used to take into account the spectral dependence of radiation transfer. The regions of partial transparency and opaque regions in the material are divided here into N_{t} and N_{o} spectral intervals, respectively: $[\bar{\nu}_a, \bar{\nu}_{a+1}]$, $a = \overline{1, N_{\mathrm{t}}}$, $[\bar{\nu}_b, \bar{\nu}_{b+1}]$, $b = \overline{1, N_{\mathrm{o}}}$. Within each spectral interval the optical properties are assumed to be independent of frequency. The integral characteristics (q_{r}, q_{v}) are determined by summing up the corresponding components over all the sections:

$$q_{\mathrm{r}} = \sum_{a=1}^{N_{\mathrm{t}}} q_{\mathrm{r},a} ; \quad q_{\mathrm{v}} = \sum_{a=1}^{N_{\mathrm{t}}} q_{\mathrm{v},a} .$$

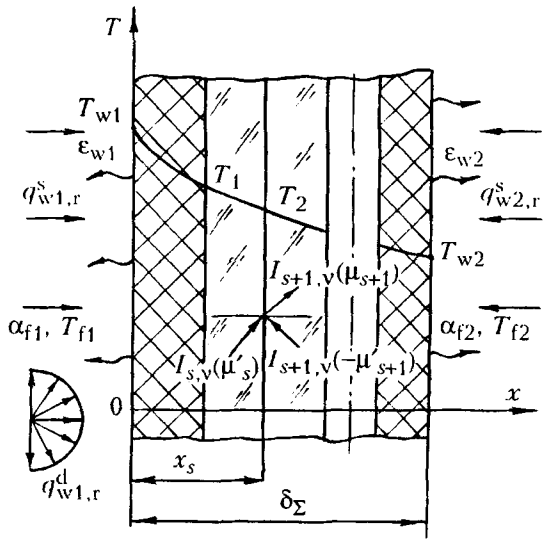

Fig. 3. Model of radiative-conductive heat exchange in a multilayer plate.

The function $B^*_\nu(T)$ in (10) is calculated by the formula $B^*_\nu(T) = 4n^2_\nu B_\nu(T)$, where $B_\nu(T) = \sigma_\nu T^4$ is the Planck function. In numerical implementation $\sigma_\nu = \sigma_0(\sigma(X_{a+1}) - \sigma(X_a))$, $a = \overline{1, N_t}$, $X = h\nu/kT^3$, and $\sigma(X)$ is approximated by the relations [17]

when $X \le 2$, $\sigma(X) = X^3(1/3 - X/8 + X^2/62.4)/6.4939$;

when $X > 2$, $\sigma(X) = 1 - \exp(-X)(X^3 + 3X^2 + 6X + 7.28)/6.4939$.

The algorithm of solution of (1)-(3), (10), and (11) is constructed on the basis of the finite-difference method. The system of nonlinear equations, obtained as a result of approximation of the differential operators of problem (1)-(3), (10), and (11) by difference ones with order of accuracy $O(\Delta\tau + \Delta x^2)$, is solved by the trial-run method with the use of iterations.

Multilayer plate with an arbitrary combination of layers of opaque and partially transparent materials (Fig. 3):

$$C_s(T)\frac{\partial T_s}{\partial \tau} = \frac{\partial}{\partial x}\left(\lambda_s(T)\frac{\partial T_s}{\partial x}\right) + q_\nu(x_s, \tau), \quad s = \overline{1, K}; \tag{12}$$

$$\tau = 0 \quad T_s = T_{s,0}; \tag{13}$$

$$x = 0(\delta_\Sigma) \quad (\mp)\,\tilde{K}_{1(2)}\lambda_{1(K)}(T)\frac{\partial T_{1(K)}}{\partial x} = (\tilde{K}_{1(2)} - 1)\,T_{1(K)} + \tilde{\varphi}_{1(2)}; \tag{14}$$

$$x = x_s \quad -\lambda_s(T)\frac{\partial T_s}{\partial x} + q_{r,s} = -\lambda_{s+1}(T)\frac{\partial T_{s+1}}{\partial x} + q_{r,s+1}; \quad T_s = T_{s+1}; \tag{15}$$

$$\mu\frac{dI_{s,\nu}(\mu)}{dx} = -(\alpha_{s,\nu} - \beta_{s,\nu})I_{s,\nu}(\mu) + \alpha_{s,\nu}n^2_{s,\nu}\frac{B_{s,\nu}(T)}{\pi} +$$

$$+\frac{\beta_{s,\nu}}{2}\int_{-1}^{1}\tilde{\rho}_{s,\nu}(\chi)I_{s,\nu}(\mu')\,d\mu', \quad s = \overline{1, K}; \tag{16}$$

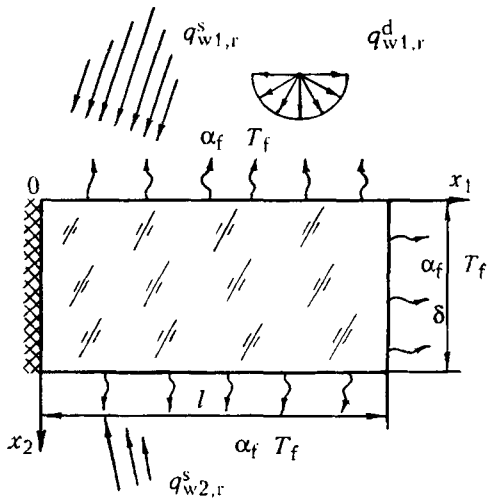

Fig. 4. Model of radiative-conductive heat exchange in a plate of limited dimensions.

$$x=0 \quad I_{1,\nu}(\mu_1)=\int_0^1 \tilde{r}_{w1,\nu}(\mu_1,-\mu_1')\, I_{1,\nu}(-\mu_1')\, d\mu_1' + \int_0^1 \tilde{q}_{w1,\nu}(\mu_1,\mu_0')\, I_{0,\nu}(\mu_0')\, d\mu_0' + \varepsilon_{w1}(\mu_1)\frac{B_{w1,\nu}(T)}{\pi}; \tag{17}$$

$$x=\delta_\Sigma \quad I_{K,\nu}(-\mu_K)=\int_0^1 \tilde{r}_{w2,\nu}(-\mu_K,\mu_K')\, I_{K,\nu}(\mu_K')\, d\mu_K' +$$

$$+\int_0^1 \tilde{q}_{w2,\nu}(-\mu_K,\mu_\delta')\, I_{K,\nu}(\mu_\delta')\, d\mu_\delta' + \varepsilon_{w2}(-\mu_K)\frac{B_{w2,\nu}(T)}{\pi}; \tag{18}$$

$$x=x_s \quad I_{s,\nu}(\mu_s)=\int_0^1 \tilde{r}_{s,\nu}(\mu_s,\mu_s')\, I_{s,\nu}(\mu_s')\, d\mu_s' +$$

$$+\int_0^1 \tilde{q}_{s+1,\nu}(\mu_s,-\mu_{s+1}')\, I_{s+1,\nu}(-\mu_{s+1}')\, d\mu_{s+1}' + \varepsilon_{s,\nu}(\mu_s)\, n^2_{s,\nu}\frac{B_{s,\nu}(T)}{\pi}; \tag{19}$$

$$I_{s+1,\nu}(\mu_{s+1})=\int_0^1 \tilde{r}_{s+1,\nu}(\mu_{s+1},-\mu_{s+1}')\, I_{s+1,\nu}(-\mu_{s+1}')\, d\mu_{s+1}' +$$

$$+\int_0^1 \tilde{q}_{s,\nu}(\mu_{s+1},\mu_s')\, I_{s,\nu}(\mu_s')\, d\mu_s' + \varepsilon_{s,\nu}(\mu_{s+1})\, n^2_{s,\nu}\frac{B_{s,\nu}(T)}{\pi},$$

where

$$q_{\nu,s}=-\frac{\partial}{\partial x}\int_{\bar{\nu}_t} q_{r,s,\nu}\, d\nu; \quad q_{r,s,\nu}=2\pi\int_{-1}^{1} I_{s,\nu}\,\mu\, d\mu .$$

The system of equations (16)-(19) is transformed using a two-term approximation of the method of moments. The averaged volumetric intensity of radiation M_0 is normalized according to the recommendations of [18]. To solve the system of finite-difference equations, set up by an implicit scheme, a data-flow variant of the trial-run method and iterations by Newton's method are used.

Plane layer of limited dimensions with inclusions (Fig. 4):

$$C_s(T)\frac{\partial T_s}{\partial \tau}=\frac{\partial}{\partial x_1}\left(\lambda_{x_1,s}(T)\frac{\partial T_s}{\partial x_1}\right)+\frac{\partial}{\partial x_2}\left(\lambda_{x_2,s}(T)\frac{\partial T_s}{\partial x_2}\right)+q_{v,s}(x_1,x_2,\tau); \tag{20}$$

$$\tau=0 \quad T_s=T_{0,s}(x_1,x_2); \tag{21}$$

$$x_1=0,l \quad \frac{\partial T_s}{\partial x_1}=0; \tag{22}$$

$$x_2=0(\delta) \quad (\bar{+})\,\tilde{K}_{1(2)}\lambda_{x_2,1(K)}(T)\frac{\partial T_{1(K)}}{\partial x_2}=(\tilde{K}_{1(2)}-1)T_{1(K)}+\tilde{\varphi}_{1(2)}, \tag{23}$$

$$\sqrt{1-\gamma^2}\left(\mu\frac{\partial I_{s,\nu}}{\partial x_1}+\sqrt{1-\mu^2}\frac{\partial I_{s,\nu}}{\partial x_2}\right)=-(\alpha_{s,\nu}+\beta_{s,\nu})I_{s,\nu}+\alpha_{s,\nu}n_{s,\nu}^2\frac{B_{s,\nu}(T)}{\pi}+$$

$$+\frac{\beta_{s,\nu}}{4\pi}\int_0^{2\pi}\int_{-1}^{1}I_{s,\nu}\tilde{\rho}(\chi)\,d\mu'd\gamma'; \tag{24}$$

$$x_1=0 \quad I_{s,\nu}(\mu,\gamma)=I_{s,\nu}(-\mu,-\gamma); \tag{25}$$

$$x_l=l \quad I_{s,\nu}(-\mu,-\gamma)=I_{s,\nu}(\mu,\gamma); \tag{26}$$

$$x_2=0 \quad I_{1,\nu}(\mu,\gamma)=\int_0^{2\pi}\int_0^{1}\tilde{r}_{w1,\nu}(\mu,-\mu',\gamma,-\gamma')I_{1,\nu}(-\mu',-\gamma')\,d\mu'd\gamma'+$$

$$+\int_0^{2\pi}\int_0^{1}\tilde{q}_{w1,\nu}(\mu,\mu_0',\gamma,\gamma_0')I_{1,\nu}(\mu_0',\gamma_0')\,d\mu_0'd\gamma_0'+\varepsilon_{w1,\nu}(\mu,\gamma)\frac{B_{w1,\nu}(T)}{\pi}; \tag{27}$$

$$x_2=\delta \quad I_{K,\nu}(-\mu,-\gamma)=\int_0^{2\pi}\int_0^{1}\tilde{r}_{w2,\nu}(-\mu,\mu',-\gamma,\gamma')I_{K,\nu}(\mu',\gamma')\,d\mu'd\gamma'+$$

$$+\int_0^{2\pi}\int_0^{1}\tilde{q}_{w2,\nu}(-\mu,\mu_\delta',\gamma,\gamma_\delta')I_{K,\nu}(\mu_\delta',\gamma_\delta')\,d\mu_\delta'd\gamma_\delta'+\varepsilon_{w2,\nu}(-\mu,-\gamma)\frac{B_{w2,\nu}(T)}{\pi}, \tag{28}$$

where

$$q_{v,s} = -\frac{\partial}{\partial x_1}\int\limits_{\bar{\nu}_t} q_{r,s,\nu}\, d\nu - \frac{\partial}{\partial x_2}\int\limits_{\bar{\nu}_t} q_{r,s,\nu}\, d\nu\,; \quad q_{r,s,\nu} = \sqrt{q_{r1,s,\nu} + q_{r2,s,\nu}}\,;$$

$$q_{r1,s,\nu} = \int\limits_{-1}^{1} \frac{\mu d\mu}{\sqrt{1-\mu^2}} \int\limits_{-1}^{1} \sqrt{1-\gamma^2}\, I_{s,\nu}\, d\gamma\,; \quad q_{r2,s,\nu} = \int\limits_{-1}^{1} d\mu \int\limits_{-1}^{1} \sqrt{1-\gamma^2}\, I_{s,\nu}\, d\gamma\,.$$

In Eq. (23), $\tilde{\varphi}_{1(2)} = \tilde{\varphi}(T, \tau, x_1)$. Below the subscripts ν and s are omitted.

To solve problem (23)-(28), the similarity transformation [19] is used, which makes it possible to reduce the problem of anisotropic scattering to an isotropic one, considering it in the new coordinates $x_{1*} = (1 - \omega a_1/3)x_1$; $x_{2*} = (1 - \omega a_1/3)x_2$. Here a_1 is the first coefficient of expansion of the shape of the scattering indicatrix in Legendre polynomials.

In the transformed coordinate system the albedo $\omega = \beta/(\alpha+\beta)$ has the form $\omega_* = \omega(1 - a_1/3)/(1 - \omega a_1/3)$, and the scattering indicatrix is considered to be spherical, $\tilde{\rho}(\chi) = 1$.

On the assumption that $\omega_* = \beta_*/(\alpha + \beta_*)$, Eq. (24) is represented in the form

$$\sqrt{1-\gamma^2}\left(\mu\frac{\partial I}{\partial x_{1*}} + \sqrt{1-\mu^2}\frac{\partial I}{\partial x_{2*}}\right) = -(\alpha+\beta_*)\, I + \alpha n^2 \frac{B(T)}{\pi} +$$

$$+ \frac{\beta_*}{4\pi}\int\limits_0^{2\pi}\int\limits_{-1}^{1} I(\mu', \gamma')\,\tilde{\rho}(\chi)\,\mu' d\gamma'\,. \tag{29}$$

Equation (29) is solved by the method of moments. The transformed system of equations is

$$\frac{\partial}{\partial x_{1*}}\left(\frac{1}{\kappa_*}\frac{\partial M_0}{\partial x_{1*}}\right) + \frac{\partial}{\partial x_{2*}}\left(\frac{1}{\kappa_*}\frac{\partial M_0}{\partial x_{2*}}\right) - 3\alpha M_0 = 3\alpha B^*(T)\,; \tag{30}$$

$$x_1 = 0, l \quad \frac{\partial M_0}{\partial x_{1*}} = 0\,; \tag{31}$$

$$x_2 = 0\,(\delta) \quad (\mp)\frac{1}{2\kappa_*}\left(\frac{1}{3} + \tilde{R}_{11w1(2)}\right)\frac{\partial M_0}{\partial x_{2*}} + \frac{1}{2}\left(\frac{1}{2} - \tilde{R}_{01w1(2)}\right)M_0 =$$

$$= q_{w1(2),r}(\tau)\,(2\eta^{d}_{w1(2)}\,\tilde{Q}_{01,w1(2)} + \eta^{s}_{w1(2)}\,\tilde{Q}_{1,w1(2)}) + 2\tilde{E}_{w1(2)}\, n^2 B_{w1(2)}(T)\,. \tag{32}$$

The spectral dependence of radiation transfer is taken into account by means of multigroup approximation. The algorithm of the transformed problem of RCHE, Eqs. (20)-(23) and (30)-(32), is constructed on the basis of numerical methods. The heat conduction equation is solved with the aid of a locally one-dimensional scheme, and the radiation transfer equation by the alternately-triangular method [20].

The models presented complement each other and serve as a basis for constructing algorithms to solve inverse problems [13].

Examples of Mathematical Simulation. At the present time thermal calculations of structures made from partially transparent porous materials are primarily carried out using the models of effective thermal conductivity (ETC). However, the values of $\lambda_{eff}(T)$ obtained for materials on different experimental setups may differ several times at high temperatures because of the difference in the intensity of radiation energy transfer in different types of specimens and measuring units. Therefore, $\lambda_{eff}(T)$ can be used in thermal calculations only for conditions similar to those under which this dependence was determined. Below we present results of

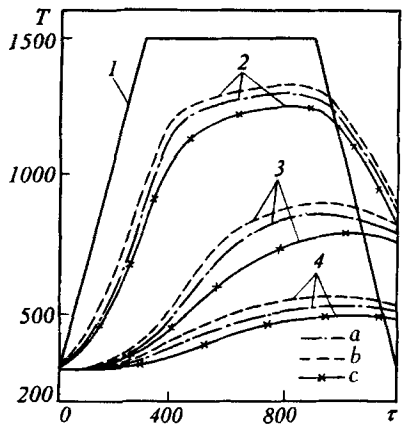

Fig. 5. Effect of the form of the temperature dependence of the thermal conductivity coefficient on the temperature state of a tiling HS: 1) T_{w1}; 2) x = 10 mm; 3) 30; 4) 40; a) RCHE model; b) $\lambda_{eff1}(T)$; c) $\lambda_{eff2}(T)$. T, K; τ, sec.

mathematical simulation that characterize the influence of the inconsistency of experimental data on $\lambda_{eff}(T)$ for high-temperature insulators on the heating of HSs. As an example we used data on TZMK-10 material, which is a sintered composition, made from high-purity quartz glass fibers, which is close in its properties to the American analog LI-900.

Tiling HS of the Buran aerospaceplane. The element of a tiling HS was considered in the form of a 40-mm-thick infinite plane layer from TZMK-10-type material heated in flight by the program shown in Fig. 5. It was assumed that both surfaces of the layer were covered with a thin opaque coating with emissivity $\varepsilon_{w1(2)} = 0.85$. The temperature dependence of the specific heat capacity of the material corresponded to that of quartz glass [21], the density was equal to 144 kg/m^3, and the temperature dependence of the molecular coefficient of thermal conductivity was assigned in the form of $\lambda(T) = 0.05 + 10^{-4}(T - 300)$ W/(m·K). The volumetric optical properties were assumed to be as follows: $\alpha = 0.5$ m^{-1}, $\beta = 7 \cdot 10^3$ m^{-1}, and $n = 1.03$. The initial temperature distribution was assumed to be uniform and equal to 293 K. Calculations were carried out on a grid with Δx = 1 mm and $\Delta\tau$ = 1 sec.

The results of mathematical simulation are shown in Fig. 5. The thermograms corresponding to the conditions of flight were determined from the RCHE model for an infinitely extended plane layer and were considered to be basic ones. Calculations by the ETC model were conducted for two variants of $\lambda_{eff}(T)$ [9]. It was assumed that $\lambda_{eff1}(T)$ was determined under the conditions of stationary heat exchange of the specimen on a setup of the "Khrustal'" Science and Production Center Corporation [22] and $\lambda_{eff2}(T)$ under the conditions of substantially nonstationary heat exchange of the specimen on the SGU-6 solar power plant of the Institute of Materials Science of the National Academy of Sciences of the Ukraine [23].

As is seen from Fig. 5, for $\lambda_{eff1}(T)$ the maximum difference from the basic variant is observed at 30 mm from the heated surface and is equal to 35–40 K, whereas on the rear surface it does not exceed 20 K. The difference of the calculated thermograms for $\lambda_{eff2}(T)$ from the basic ones is more significant and comes to 100 K at a depth of 30 mm from the heated surface and to 60 K on the rear surface. The use of the function $\lambda_{eff1}(T)$ in thermal calculations leads to smaller differences from the basic variant than for the dependence with $\lambda_{eff2}(T)$, since the experimental conditions for heat exchange of the specimen on setups such as the one at the "Khrustal'" Science and Production Center Corporation ($\partial T/\partial\tau = 0$; $\partial T/\partial x$ = 1 K/mm) are closer to those of flight ($\partial T/\partial\tau$ = 4 K/sec) than to the conditions which are usually realized on installations of radiative heating ($\partial T/\partial\tau$ up to 200 K/sec; $\partial T/\partial x$ up to 1000 K/mm).

HS of a promising SSTS. It is assumed that promising SSTSs will use multilayer HSs constructed as an integrated circuit which unites the load-bearing structures of the body and cryogenic tank with heat insulations for different temperature ranges of operation [1].

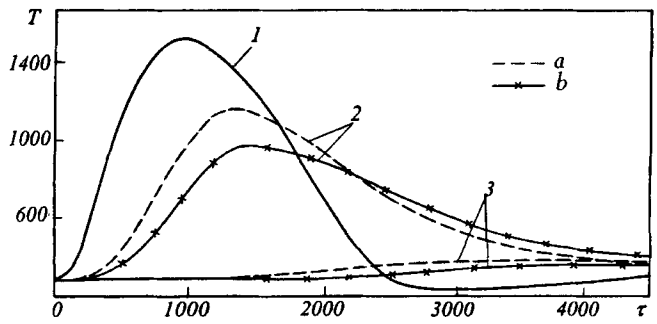

Fig. 6. Change in the temperature state of the HS of a promising SSRS (ETC model): 1) T_{w1}; 2) T_2 (x= 33 mm); 3) T_{w2} (x = 228 mm); a) $\lambda_{eff1}(T)$; b) $\lambda_{eff2}(T)$.

TABLE 2. Initial Data for Simulating the Temperature State of the HS of a Promising SSTS

Heat transfer parameters	Number of layer	
	2	3
ρ, kg/m^3	144	30
C, J/(m^3·K)	$172 + 1.28T - 2.4\cdot10^{-5}T^2$	$705 + 0.17T - 5.3\cdot10^{-5}T^2$
λ, W/(m·K)	$0.04 + 3.7\cdot10^{-5}T + 2.5\cdot10^{-8}T^2$	$0.04 + 3.7\cdot10^{-5}T + 1.1\cdot10^{-8}T^2$
λ_{eff1}, W/(m·K)	$0.017 + 1.2\cdot10^{-4}T + 6.8\cdot10^{-8}T^2$	$0.018 + 2.5\cdot10^{-4}T + 1.7\cdot10^{-7}T^2$
λ_{eff2}, W/(m·K)	$0.04 + 3.7\cdot10^{-5}T + 3.5\cdot10^{-8}T^2$	$0.4 + 3.7\cdot10^{-5}T + 1.1\cdot10^{-8}T^2$
α, m^{-1}	0.66	0.66
β, m^{-1}	6485	7000
n	1.03	1.0

The heating of a three-layer fragment of HS was modeled under specified conditions of the change in temperature on the frontal surface $T_{w1}(\tau)$. These conditions correspond to bench tests that simulate aerodynamic heating in flight. The rear surface was assumed to be heat-insulated. The initial temperature distribution was assumed to be uniform and equal to 293 K. The following properties were imparted to the first 2-mm-thick layer of carbon-carbon composite: ρ = 1700 kg/m^3, $c_p(T) = -221 + 3.38T - 1.3\cdot10^{-3}T^2 - 9.8\cdot10^{-9}T^3$ J/(kg·K); $\lambda(T) = 50.4 - 1.5\cdot10^2T + 8.5\cdot10^7T^2$ W/(m·K), $\varepsilon_{w1(2)}$ = 0.9. It was assumed that the second layer was 31 mm thick and made from the TZMK-10-type material, and the third 195-mm-thick layer was made from glass wool. Due to the partial transparency of the materials of the second and third layers, two temperature dependences of the effective thermal conductivity coefficient were specified for each of them: $\lambda_{eff1}(T)$ corresponding to the conditions of the experiment on the setup at the "Khrustal'" Science and Production Center Corporation and $\lambda_{eff2}(T)$ characteristic of the tests on solar power plants at the Institute of Materials Science of the National Academy of Sciences of the Ukraine. To model the RCHE processes, dependences of the molecular coefficient of thermal conductivity $\lambda(T)$ were introduced; for glass wool, $\lambda(T)$ coincided with $\lambda_{eff2}(T)$. The bulk OPs of materials were considered to be independent of temperature and wavelength. A summary of the TPPs and OPs of the materials of the second and third layers is given in Table 2. Calculations were carried out on a grid with Δx = 1 mm and $\Delta\tau$ = 1 sec.

As follows from the results of calculations (Figs. 6 and 7), the temperature drop in the first layer is small, and it is admissible to assume that this layer is uniformly heated. The maximum value of the temperature T_1 coincides with the maximum temperature of the frontal surface T_{w1} = 1550 K occurring at the 960th second of flight. Because of the low thermal resistance of the carbon-carbon composite layer, the portions of

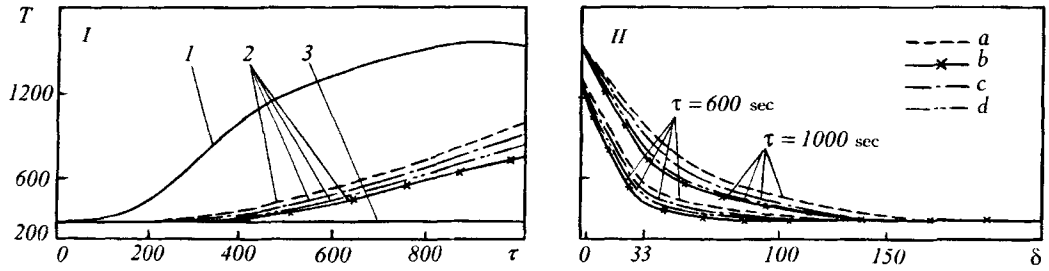

Fig. 7. Change in the temperature state of the HS of a promising SSTS in time (*I*) and over its thickness (*II*): 1) T_{w1}; 2) T_2 (x = 33 mm); 3) T_{w2} (x = 228 mm); a) $\lambda_{eff1}(T)$; b) $\lambda_{eff2}(T)$; c) RCHE model; the boundaries of the third layer are transparent; d) same, $\varepsilon_2 = \varepsilon_{w2} = 0.3$. δ, mm.

TABLE 3. Effect of the Thickness of Layers of Partially Transparent Materials and the Emissivity of the Boundaries of the Third Layer on the Temperature State of the Rear Surface of HS

T, K	$\varepsilon_2 = \varepsilon_{w2}$			
	0.1	0.3	0.5	0.9
	τ = 600 sec, T_{w1} = 1300 K			
T_2	448/557	446/553	445/552	445/551
T_{w2}	293/470	293/467	293/466	293/466
	τ = 800 sec, T_{w1} = 1445 K			
T_2	619/810	614/801	613/799	612/798
T_{w2}	293/713	293/706	293/704	293/703
	τ = 1000 sec, T_{w1} = 1532 K			
T_2	816/1082	807/1068	805/1064	804/1062
T_{w2}	293/1005	293/900	293/987	293/984

Note: The numerator δ_Σ = 228 mm; the denominator δ_Σ = 47 mm.

the second layer contacting with the first layer will work for several hundreds of seconds at temperatures that are limiting for TZMK-10, and care should be taken to replace it by another, more thermally stable material.

The temperature distribution in the second layer is characterized by large temperature gradients and to a great extent depends on the adopted dependence $\lambda_{eff}(T)$. By the 800th second of flight the temperature drop over the thickness of the second layer can reach 760 K for $\lambda_{eff}(T)$ and 910 K for $\lambda_{eff2}(T)$. According to both dependences $\lambda_{eff1}(T)$, the difference between the values for the temperature of the junction between the second and the third layers T_2 will increase with temperature, and at the 1000th second of flight may exceed 225 K. By the 1500th second of flight the temperature T_2 for the function $\lambda_{eff1}(T)$ is capable of attaining its maximum value of 1130 K, while for $\lambda_{eff2}(T)$ T_2 = 967 K. The contradictory nature of the data on $\lambda_{eff}(T)$ may be the reason for the overheating of the joint between the second and the third layers, shrinkage, and loss of insulating properties by the glass wool should T_2 exceed the admissible temperature, which is recommended to be maintained not higher than 1000 K [24]. It is noteworthy that the maximum temperature at the boundaries of the layers will be attained with delay in time. So, when $\lambda_{eff1}(T)$ is used, the maximum T_2 = 1130 K will occur at the 1500th second and the maximum T_{w2} = 398 K at the 4000th second. It is remarkable that when T_2

attains its maximum at the 1500th second, the rear surface will display signs of response to the heating of the frontal surface only weakly.

Comparing the results of calculations carried out by the RCHE and ETC models and presented in Figs. 6 and 7, it can easily be found that the former results lie in a tube formed by the thermograms obtained for $\lambda_{eff1}(T)$ and $\lambda_{eff2}(T)$. Whence it follows that the function $\lambda_{eff3}(T)$, corresponding to the conditions of flight, would have occupied an intermediate position between $\lambda_{eff1}(T)$ and $\lambda_{eff2}(T)$. The RCHE model makes it possible to analyze the role of opaque screens at the boundaries of the layers made from partially transparent materials. It has been found that with free boundaries of the third layer the temperature level over the entire thickness of the HS turns out to be higher than in the presence of opaque screens. The placement of thin-walled metal-foil screens within the HS exerts a favorable influence on the decrease in overall heat transfer to the rear surface.

When preparing thermal tests of large-scale fragments of HS, a necessity arises to find the limits of decrease in the dimensions of individual layers in order to use the available equipment.

In the case considered, with a decrease in the thickness of the third layer, the temperature at its junction with the second layer T_2 and at the rear surface T_{w2} will increase more rapidly than in a full-scale structure (Table 3). So, for a structure with the third layer of thickness 14 mm and overall thickness of 47 mm (scale 1:5) and $\varepsilon_2 = \varepsilon_{w2} = 0.1$, the difference between T_2 of the natural object and the model at the 600th second of tests will come to 109 K and between T_{w2} of the natural object and the model to about 177 K, and 200 sec later the difference between T_2 of the natural object and the model may attain 266 K and between T_{w2} of the natural object and the model may increase to 712 K. The difference in the temperature fields of the full-scale structure and the model of reduced thickness turns out to be the larger, the smaller the emissivity of opaque surfaces at the boundaries of the third layer. The effect of ε_2 and ε_{w2} on T_{w2} is higher than on T_2. The revealed peculiarities point to the necessity of limiting the time of tests with the object model and the zone of measurement by the layers adjoining the frontal surface, where the conditions of heat exchange on the rear surface have a weak effect.

Thus, the use of RCHE models is an effective means of increasing the accuracy of design and experimental verification of SSTS HSs.

The author expresses his gratitude to his colleagues D. Yu. Kalinin, A. A. Mikhalev, P. V. Prosuntsov, and I. G. Plokhotin for useful discussions of the problems raised in the present work.

The work was carried out with financial support from the Ministry of Education of the Russian Federation (grants in the field of rocket-space thermal engineering for 1997-2000) and from INTAS (code of the project 94-700/701).

NOTATION

T, temperature; τ, time; I, radiation intensity; x, x_1, and x_2, coordinate axes; δ, l, thickness and width of the plate; R, radius of the solid cylinder; R_1 and R_2, internal and external radii of the hollow cylinder; Δx, $\Delta\tau$, steps in space and time; q_v, internal heat sources; q, heat flux density; α_t, heat transfer coefficient; C, volumetric heat capacity; c_p, specific heat capacity; λ, thermal conductivity coefficient; Ω, solid angle; $\tilde{\rho}(\chi)$, scattering indicatrix; χ, angle of scattering, for the plate $\chi = (\mu, \mu')$, for the cylinder $\chi = (\mu, \gamma, \mu', \gamma')$; α_v, absorption coefficient; β, scattering coefficient; $\kappa = \alpha + \beta(1 - p)$, attenuation coefficient; p, parameter of the scattering indicatrix which has Henji–Greenstein's form $\tilde{\rho}(\chi) = (1 - p^2)/(1 + p^2 - 2p\cos\chi)^{3/2}$; $\bar{\omega} = \beta/(\alpha + \beta)$, scattering albedo; n, refractive index; A, absorptivity; ε, emissivity; $\tilde{r}$, indicatrix of reflection of the boundary surface; $\tilde{q}$, indicatrix of transmission of the boundary surface; $I(\mu)$, $I(\mu')$, and $I(\mu, \gamma)$, $I(\mu', \gamma)$, radiation intensities in the primary direction of radiation propagation and in the direction of scattering; $\mu'^s = \cos\vartheta_0^s$, ϑ_0^s, angle of incidence of directional radiation from the external source; $\mu = \cos\vartheta$, $\gamma = \cos\psi$, and also μ_0', μ_0, $-\mu'$, μ', $-\mu$, μ_δ', μ_δ, γ_0', γ_0, $-\gamma'$, γ', $-\gamma$, γ_δ', γ_δ, directing cosines; $\mu^* = \sqrt{n^2 - 1}/n$, cosine of the angle of complete internal reflection; $B_\nu^* = 4n_\nu^2 B_\nu(T)$; $X = \hbar\nu/kT^3$, $\hbar = 6.62\cdot10^{-34}$ J·sec, Planck's constant; $k = 1.38\cdot10^{-23}$ J/K, Boltzmann's constant; $\sigma_0 = 5.67\cdot10^{-8}$ W/(m$^2\cdot$ K^4), Stefan–Boltzmann constant; I^d and I^s, con-

stant components of the diffuse and directional constituents of radiation of the external sources; b_j, coefficients of expansion of the diffuse constituent in a power series; J, number of series terms; $\tilde{\delta}(\mu'_{0(\delta)} - \mu^3_{0(\delta)})$, Dirac delta-function; M_0, moment of intensity of zero order; $\tilde{R}_{\tilde{m}\tilde{n}}$, $\tilde{Q}_{\tilde{m}.\tilde{n}}$, $\tilde{Q}_{\tilde{m}}$, and $\tilde{E}$, integral optical characteristics of the boundary surfaces; $\bar{n}$, quantity characterizing the shape of the object investigated: $\bar{n} = 0$, plate, $\bar{n} = 1$, cylinder; $\tilde{K}$, quantity indicating the type of boundary conditions: $\tilde{K} = 0$, boundary conditions of the first kind, $\tilde{K} = 1$, boundary conditions of the second and third kind, or mixed ones; $\tilde{\varphi}$, coefficient describing conditions of heat balance on the surface; ν, frequency; $\bar{\nu}_t$, $[\bar{\nu}_a, \bar{\nu}_{a+1}]$, spectral interval of partial transparency of material; N_t, number of spectral intervals of partial transparency of material; $\bar{\nu}_o$, $[\bar{\nu}_b, \bar{\nu}_{b+1}]$, spectral interval of opaqueness of material; N_o, number of spectral intervals of opaqueness of material; η^d, η^s, fractions of diffuse and directional constituents of radiation; $x_{1*} = (1 - \omega a_1/3)x_1$, $x_{2*} = (1 - \omega a_1/3)x_2$, system of coordinates obtained as a result of similarity transformation; a_1, first coefficient of expansion in Legendre polynomials of the form of the scattering indicatrix; K, number of layers. Subscripts: 0, initial value; eff, effective value; s, number of a layer; w, wall; f, surrounding fluid (gas or liquid); 1(2) and 0(δ), frontal (rear) surface of the wall; v, volumetric; r, radiant; t, partially transparent; o, opaque; a, $a + 1$, limits of the spectral interval of partial transparency; b, $b + 1$, limits of the spectral interval of transparency. Superscripts: d, diffusion flux of radiation; s, directional radiation flux. $\tilde{m}, \tilde{n} = 0, 1, 2, \ldots$, integer indices of moment transformation.

REFERENCES

1. H. N. Kelly, D. R. Rummler, and L. R. Jackson, *AIAA/NASA Conf. Adv. Technol. Future Space Syst.: Collection Techn. Pap. S. I.*, s.a. Hampton (Va.) (1979), pp. 12-23.
2. P. A. Cooper and P. F. Holloway, *Astronautics Aeronautics*, **19**, No. 1, 24-34 (1981).
3. D. Chaumette and J. Cretenet, *Acta Astronaut.*, **16**, No. 3, 391-399 (1987).
4. G. E. Lozino-Lozinskii, in: *Gagarin Scientific Readings on Astronautics and Aviation in 1989* [in Russian], Moscow (1990), pp. 6-21.
5. V. P. Timoshenko, in: *Advanced Thermal Technologies and Materials* [in Russian], Pt. 2, Moscow (1999), pp. 11-16.
6. B. M. Pankratov, Yu. V. Polezhaev, and A. K. Rud'ko, *Interaction of Materials with Gas Streams* [in Russian], Moscow (1976).
7. O. M. Alifanov, B. P. Gerasimov, T. G. Elizarova, et al., *Inzh.-Fiz. Zh.*, **49**, No. 5, 781-791 (1985).
8. O. M. Alifanov, N. A. Bozhkov, V. K. Zantsev, and S. N. Obruch, in: *Gagarin Scientific Readings on Aviation and Astronautics in 1988* [in Russian], Moscow (1989), pp. 19-26.
9. P. V. Prosuntsov and S. V. Reznik, in: *Gagarin Scientific Readings in Astronautics and Aviation in 1989* [in Russian], Moscow (1990), pp. 56-60.
10. G. A. Kiselev, O. A. Gladkikh, O. A. Makhotkin, and S. A. Gusev, in: *Abstr. 8th All-Union Conf. on Thermophys. Properties of Substances* [in Russian], Novosibirsk (1988), pp. 198-199.
11. A. V. Kondratenko, S. S. Moiseev, V. A. Petrov, and S. V. Stepanov, *Teplofiz. Vys. Temp.*, **29**, No. 1, 134-138 (1991).
12. A. V. Galaktionov, V. A. Petrov, and S. V. Stepanov, *Teplofiz. Vys. Temp.*, **32**, No. 3, 398-405 (1994).
13. S. V. Reznik, in: *Proc. 3rd Minsk Int. Forum "Heat and Mass Exchange–MIF-96,"* Minsk, May 20-24, 1996 [in Russian], Vol. 2, Minsk (1996), pp. 141-149.
14. M. Krook, *Astrophysical J.*, **122**, No. 3, 488-497 (1955).
15. V. V. Gorskii and V. A. Tovstonog, in: *Thermal Regime of Structures of Semitransparent Materials (Tr. MVTU*, No. 205) [in Russian], Moscow (1976), pp. 70-78.
16. V. N. Eliseev and V. A. Tovstonog, *Theoretical Foundation of Calculation of Complex Heat Exchange in Structural Elements* [in Russian], Pt. 1, Moscow (1982).
17. B. N. Chetverushkin, *Mathematical Simulation of the Problems of Radiant Gas Dynamics* [in Russian], Moscow (1985).
18. A. V. Galaktionov and S. V. Stepanov, *Teplofiz. Vys. Temp.*, **26**, No. 5, 940-946 (1988).

19. H. Lee and R. O. Bakius, *Heat Transfer* [Russian translation], **104**, No. 1, 74-82 (1982).
20. A. B. Kucherov and E. S. Nikolaev, *Zh. Vych. Mat. Mat. Fiz.*, **16**, No. 5, 1164-1174 (1976).
21. O. A. Sergeev and A. G. Shashkov, *Thermophysics of Optical Media* [in Russian], Minsk (1983).
22. V. E. Tyutyunnik, in: *Production and Investigation of Glass and Silicate Materials* (Sborn. nauch. trudov GF GIS No. 6) [in Russian], Yaroslavl (1978).
23. V. S. Dvernyakov, *Kinetics of High-Temperature Damage to Materials* [in Russian], Kiev (1981).
24. N. V. Bol'shakova, K. S. Borisanova, V. I. Burtsev, et al., *Materials for Electrothermal Installations: Handbook* [in Russian], Moscow (1987).